Journal of Hazardous Materials 515 (2026) 143175

Contents lists available at ScienceDirect

Journal of Hazardous Materials

journal homepage: www.elsevier.com/locate/jhazmat

Microplastic incorporation into soil aggregates of arable land

Max Groß [a,b,*], Melanie Braun [b], Johannes Leonhardt [c], Christina Bogner [d], Rafaela Debastiani [e,f], Larissa Hennig [a], Rachel Hurley [g], Matthias Mail [e,f,h], Virtudes Martínez-Hernández [i], Luca Nizzetto [g], Ribana Roscher [c], Paula E. Redondo-Hasselerharm [i], Torsten Scherer [e,f], Vera Schlierenkamp [d], Salla Selonen [j], Helena Soinne [k], Wulf Amelung [a]

[a] Institute of Crop Science and Resource Conservation (INRES), Soil Science and Soil Ecology, University of Bonn, Nussallee 13, Bonn 53115, Germany
[b] Institute of Crop Science and Resource Conservation (INRES), Soil Protection and Ecosystem Health, University of BonnNussallee 13, Bonn 53115, Germany
[c] Machine Learning in Agriculture, Institute of Geodesy and Geoinformation, University of Bonn, Niebuhrstr. 1a, Bonn 53113, Germany
[d] Ecosystem Research Group, Institute of Geography, Faculty of Mathematics and Natural Sciences, University of Cologne, Zülpicher Straße 45, Cologne 50674, Germany
[e] Institute of Nanotechnology (INT), Karlsruhe Institute of Technology (KIT), Hermann-von-Helmholtz-Platz 1, Eggenstein-Leopoldshafen, 76344, Germany
[f] Karlsruhe Nano Micro Facility (KNMFi), Karlsruhe Institute of Technology (KIT), Hermann-von-Helmholtz-Platz 1, Eggenstein-Leopoldshafen, 76344, Germany
[g] Norwegian Institute for Water Research (NIVA), Økernveien 94, Oslo 0579, Norway
[h] Tescan GmbH, Zum Lonnenhohl 46, Dortmund 44319, Germany
[i] IMDEA Water Institute, Avda. Punto Com 2, Alcalá de Henares 28805, Spain
[j] Finnish Environment Institute, Latokartanonkaari 11, Helsinki 00790, Finland
[k] Natural Resources Institute Finland (Luke), Latokartanonkaari 9, Helsinki 00790, Finland

HIGHLIGHTS

- Field experiment conducted in Finland, Germany and Spain over two growing seasons.
- Up to 65% of LLDPE MPs and 76% of PBAT/starch MPs were occluded in soil aggregates.
- Occlusion increased over time for both polymers.
- Free and occluded MP differed in morphology.

GRAPHICAL ABSTRACT

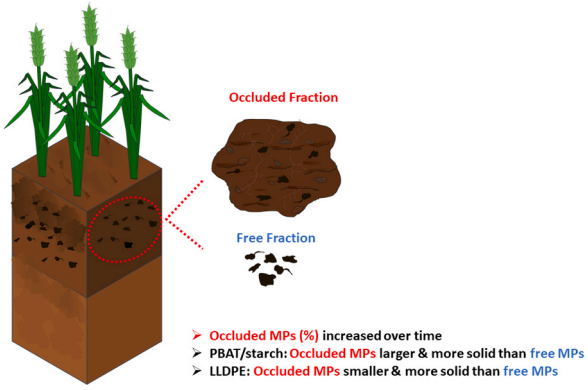

ARTICLE INFO

Keywords:
Biodegradable plastics
Mulch film

ABSTRACT

Agricultural mulch films are widely applied to increase crop productivity but are a significant source of microplastics (MPs) in the environment. We investigated the incorporation of conventional and biodegradable MPs into soil aggregates from agricultural fields in Finland, Germany and Spain, hypothesising that (i) MPs

* Corresponding author at: Institute of Crop Science and Resource Conservation (INRES), Soil Science and Soil Ecology, University of Bonn, Nussallee 13, Bonn 53115, Germany.
E-mail address: max.gross@uni-bonn.de (M. Groß).

https://doi.org/10.1016/j.jhazmat.2026.143175
Received 13 May 2026; Received in revised form 1 July 2026; Accepted 1 August 2026
Available online 2 August 2026

Field experiment
Scanning electron microscopy
Aggregate occlusion

become increasingly occluded within soil aggregates over time, (ii) the extent of occlusion differs between conventional and biodegradable MPs, and (iii) occluded MPs differ in morphology and surface characteristics from free MPs. Arable fields were spiked with MPs derived from either a biodegradable polybutylene adipate terephthalate-starch blend (PBAT/starch) or conventional linear low-density polyethylene (LLDPE) mulch films. Soil samples were collected after two barley-growing seasons, separated into free and occluded fractions, and analysed using digital microscopy and deep learning to quantify MP abundance, size and shape. Surface properties were assessed using scanning electron microscopy.

Total MP abundance declined between cropping seasons for both polymer types, while the proportion of aggregate-occluded MPs increased, reaching 76% for PBAT/starch and 65% for LLDPE. Soil exposure altered the size, shape and surface properties of MPs in a polymer-specific manner. Occluded PBAT/starch MPs were larger and more solid than their free counterparts, consistent with protection against weathering and fragmentation within aggregates. Occluded LLDPE MPs were smaller than free particles but also exhibited higher solidity, likely reflecting preferential incorporation of particles with smoother, more uniform edges. We conclude that soil aggregate occlusion is a key mechanism governing MP fate in agricultural soils, promoting particle stability while simultaneously reducing mobility and bioavailability.

1. Introduction

Plastic pollution is ubiquitous, and soils are considered to be the world's largest reservoir of plastic waste [1]. Plastics in soil are typically introduced through the application of soil amendments such as compost, biogas residues, sludge or wastewater irrigation. However, they can also result from the direct use of plastics in agricultural practices, such as plastic strings, drip irrigation pipes, greenhouses, and mulch films [2–4]. The latter, typically made of low-density polyethylene, enhances crop productivity by suppressing weeds, regulating soil temperature and moisture, and preventing soil erosion [5,6]. Conventional plastic films typically remain on the soil surface for a few months to 4 years, depending on their thickness, the presence of stabilizing additives and the cultivated crop, before they are removed and replaced [7,8].

During this period, weathering and degradation processes drive the fragmentation of conventional mulch films into micro- and submicron plastics [9,10]. For low-density polyethylene, photo-oxidation is a key process, in which impurities in the polymer structure act as initiation points for chain scission and cross-linking under UV radiation [11,12]. Additionally, mechanical forces caused by abrasion from soil particles, as well as soil cultivation practices, promote physical fragmentation [13]. As low-density polyethylene is hardly susceptible to biodegradation, the total carbon mass of conventional MPs in soil remains largely constant while the particles progressively disintegrate into smaller fragments [11,14]. Hence, the concentration of MPs in soil typically increases with the duration of plastic mulching, while their size progressively decreases [15,16].

The recycling and reuse of conventional mulch films is both costly and technically challenging, not only due to the fragmentation processes, but also due to contamination with agrochemicals, soil minerals, and organic matter [6,17]. As an alternative, biodegradable mulch films have been introduced in recent years. They commonly comprise starch blends, polybutylene adipate terephthalate (PBAT), polybutylene succinate (PBS), poly(ε-caprolactone) (PCL), polylactic acid (PLA), and polyhydroxy alkanoate (PHA), aliphatic-aromatic copolyesters (AAC), cellulose, and protein-based polymers [18]. Unlike conventional mulch films, biodegradable mulch films are designed to fully degrade to CO_2, water and biomass in soil once their service life has ended, thus avoiding long-term contamination by plastic waste [6,19]. PBAT is specifically susceptible to microbial enzymatic activity, hydrolysis and thermal degradation; the blending with hydrophilic starch further accelerates breakdown by increasing water diffusivity within the polymer matrix [20,21]. However, these degradation processes require sufficient soil moisture, temperature and microbial activity, and are frequently incomplete under field conditions [6,22–24]. In consequence, biodegradable plastics bear the risk of fragmenting even more readily into smaller pieces than conventional mulch films, thus also posing environmental risks [18]. In contrast to conventional plastics, however, biodegradation leads to an actual reduction in total polymer mass over time rather than merely a fragmentation into smaller particles [25].

The resulting MP particles in soil may participate in various natural processes, including vertical transport and incorporation into soil aggregates. Smaller MPs exhibit higher mobility in soil compared to larger particles, with transport rates depending on particle size and soil pore size distribution, the latter affected by soil properties such as texture [26,27]. Vertical transport into deeper soil layers may occur through preferential flow paths facilitated by rainfall and infiltration, as well as through bioturbation by soil fauna such as earthworms [4,28]. Beyond vertical transport, MPs may also interact with soil aggregates similarly to plant-derived particulate organic matter (POM). Soil aggregates, formed through the interaction of soil minerals, organic matter, and microbial binding agents, represent a fundamental organisational unit of soil structure [29,30]. Within this structure, POM can become encrusted with minerals or become occluded within soil aggregates, which makes it less bioaccessible and, consequently, protects it from rapid decomposition [29–31]. Similarly, MPs might take part in soil aggregation processes [32], which, if this occurs, will significantly prolong the residence time of MPs in soil.

The possibility of an occlusion of MPs into soil aggregates has already been shown by a few studies; however, the driving factors for aggregate occlusion of MPs are not yet known. As soil properties such as soil organic matter or clay content promote soil aggregate formation [33], it seems reasonable that these soil properties also promote the occlusion of MPs in soil aggregates. Further, the extent to which MPs are occluded in soil aggregates likely depends on MP concentration, form, size, and also polymer type [34,35]. For instance, Lehmann et al. [34] demonstrated under laboratory conditions that PE and polyethylene terephthalate, in particular, influenced aggregate formation, which was proposed to be linked to the leaching of polymer-specific additives. Under environmental conditions, a large percentage of MPs can be incorporated into soil aggregates. For instance, Zhang & Liu [7] found that 72% of MPs in Chinese greenhouse soils (Nitisol and Gleysol) were occluded in soil aggregates, with most particles being incorporated into large macroaggregates (>2 mm). Also, in soils across different land use types, the highest concentrations of MPs were consistently found in the largest aggregate fraction (>5 mm) in the top 20 cm of soils in the Loess Plateau terraces of China [36]. Hence, protection of MPs within soil aggregates may significantly delay their decomposition; however, the rates at which MPs are occluded in soil aggregates, how this occlusion changes over time and with the cropping season, and the factors affecting the aggregate occlusion are still unknown.

The main objective of this study was to investigate the incorporation of conventional and biodegradable MPs into soil aggregates from agricultural fields. Specifically, we hypothesized that (i) the majority of MPs become occluded within soil aggregates, and that this percentage increases over time; (ii) the extent of occlusion differs between MP types; and (iii) occluded MPs differ from free MPs in properties such as size, shape, and surface characteristics. To test these hypotheses, we sampled

experimental fields in Finland, Germany, and Spain, where soils were spiked with both conventional and biodegradable MPs. MPs were separated into free and occluded MP fractions, following the nomenclature of free and occluded POM as commonly used in soil organic matter research [31,37–39].

2. Materials and methods

2.1. Plastic particles characterization

Microplastic particles (<1 mm) were produced from recycled conventional linear low-density polyethylene (LLDPE; M-rPE-black-A0) and a biodegradable starch–PBAT blend (M-rBIO-black-A0) mulch film by cryomilling [40]. Before milling, virgin mulch films (15 µm thickness) were melted and re-extruded into pellets to simulate the processing history of recycled films and to better represent the properties of mulch films aged under field conditions. The resulting MPs contained a variety of inorganic constituents, such as cobalt, aluminium, chromium and iron, as well as organic additives including plasticisers, antioxidants and light stabilisers. A comprehensive characterisation of MP properties and composition can be found in Hurley et al. [40]. To enable comparisons with soil-exposed MPs, the size and shape parameters of the original particles were determined with a digital microscope (details in Section 2.4). For this purpose, 50–60 mg of each MP type was weighed, yielding approximately 18,000 particles for the PBAT/starch blend and 6000 particles for LLDPE. In addition, to evaluate surface characteristics, six original MPs per plastic type were prepared for scanning electron microscopy (SEM) analysis (details in Section 2.5).

2.2. Field experiment and soil sampling

The field experiments were implemented as part of the EU H2020 PAPILLONS project at three agricultural sites in Finland, Germany, and Spain, each with no history of mulch film use or biosolid application (Figure S1; Supplementary Information). The experiment started in 2022 and lasted for two barley (*Hordeum vulgare*) growing seasons until autumn 2023 (detailed description in Šmídová et al. [41]). The chosen sites differed in climatic conditions and soil texture, with sandy clay loam in Finland, silt loam in Germany, and silty-clay loam in Spain (Table S1 and Figure S2; Supplementary Information, and Šmídová et al.

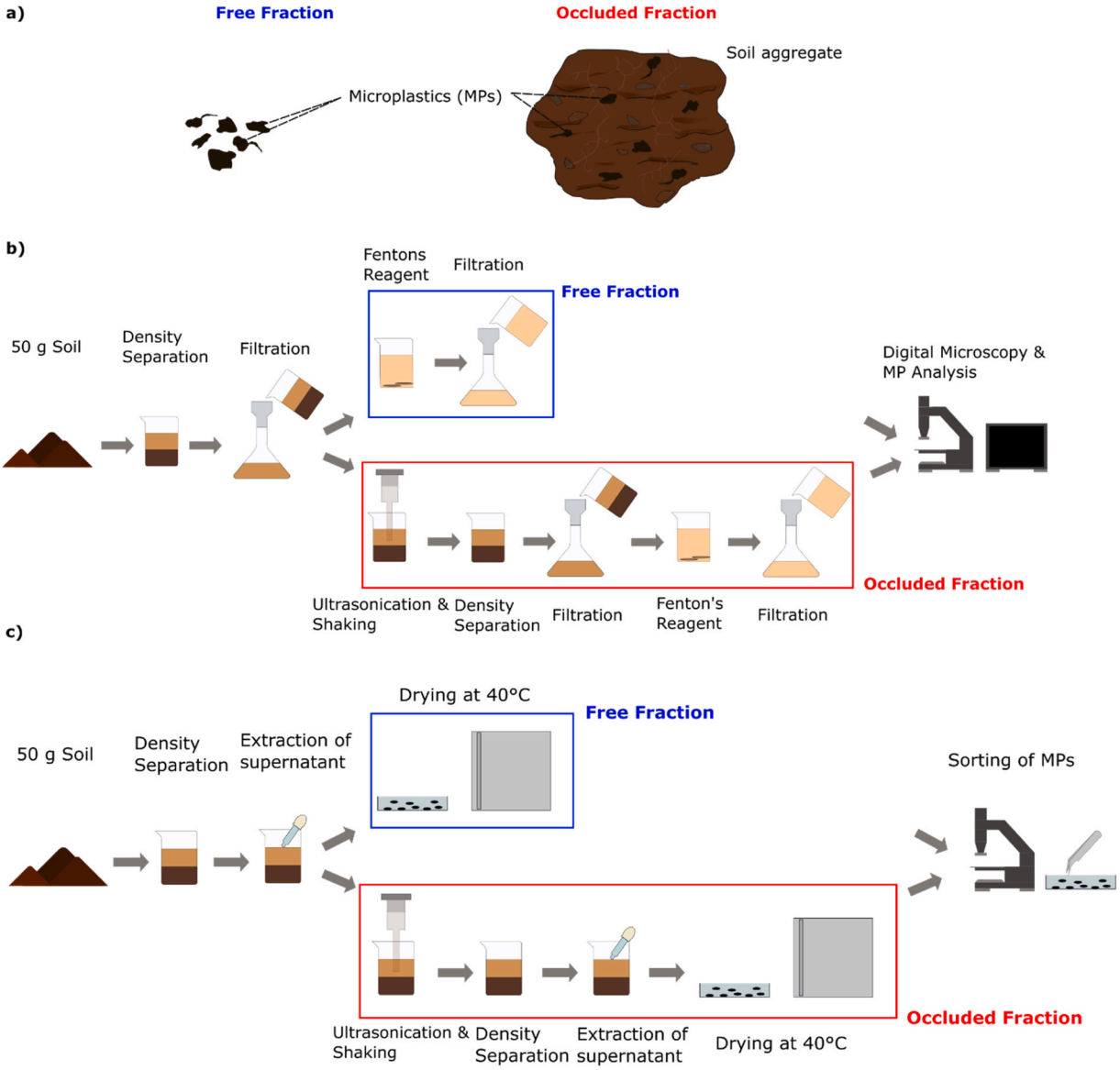

Fig. 1. Schematic representation of (a) free and aggregate-occluded microplastic particles in soil. Overview of the extraction, fractionation and analysis method for microplastic particles from soil aggregates for (b) quantification and (c) for scanning electron microscopy analysis.

[41] for further information). Unlike the gradual in situ fragmentation of mulch films, which generates plastic residues ranging from large fragments to small plastic particles, PBAT/starch and LLDPE MPs were directly applied at 0.005% and 0.05% per dry weight of soil and incorporated into the topsoil (0–10 cm) using a rotavator. This approach was chosen to track defined MPs over time and to isolate the effects of soil exposure and fragmentation on their abundance, size, shape and aggregate incorporation. Each field was divided into 25 plots (16 m^2 each) using a randomised block design with two factors: MP typology (PBAT, LLDPE) and concentration level, each replicated five times. After each growing season, topsoil (0–10 cm) samples from the LLDPE and PBAT/starch plots with 0.05% MP concentration were collected with spades to preserve the soil structure and further dried and stored at room temperature.

2.3. Microplastic extraction and analysis

Firstly, 50 g of air-dried soil per sample plot, sieved through a 5 mm mesh, was weighed into a 400 mL beaker. To extract free MP, a density separation solution, pre-filtered through a 0.2 μm glass fibre filter (MN QF−10, Macherey-Nagel), was added to each sample. The mixture was gently stirred and left to settle for 12 h. For LLDPE samples, a zinc chloride ($ZnCl_2$) solution (100 g $ZnCl_2$ dissolved in 100 mL H_2O; density: 1.6 g cm^{-3}) was used. For PBAT/starch samples, a potassium formate (KCOOH) solution of similar density (1.5 g cm^{-3}) was applied (140 g of KCOOH dissolved in 60 mL of H2O) (Fig. 1a-b). The use of different solutions was necessary, as the corrosive nature of $ZnCl_2$ might promote PBAT/starch fragmentation [42]. We did not conduct recovery experiments as the $ZnCl_2$ and potassium formate used are well-established solutions for density separation of MPs, and their recovery efficiencies have been validated in previous studies [43–46].

Approximately 300 mL of the supernatant was vacuum-filtered through a stainless-steel filter with a 10 μm pore size, and adhering particles were rinsed with deionized, pre-filtered (MN QF−10, Macherey-Nagel) H_2O. Filters were then washed with H_2O and dried at 40°C to obtain the free MP fraction.

To extract the occluded fraction, the remaining soil and solution in the beakers were adjusted to a pre-defined volume of 220 mL by adding the respective density solution. Samples were then ultrasonicated at 100 J mL^{-1} (Branson Sonifier W−250 D), transferred to 500 mL glass bottles, and shaken for 30 min at 220 rpm on a horizontal shaker. After another 12-hour settling period, the supernatant was filtered, rinsed, and dried as described above (Fig. 1).

Organic matter removal for both fractions was performed using Fenton's reagent. Filters of the respective sample and fractions were placed in a beaker and treated with 25 mL Fe(II) solution (0.05 M), 25 mL H_2O, and 25 mL of 35% H_2O_2. The reaction was monitored for four hours, with additional H_2O_2 added if required. Once decomposition was complete, 300 mL of H_2O was added to stop the reaction, followed by a final 12-hour settling period. The solution was vacuum-filtered again, rinsed with H_2O, and dried at 40 °C. Microscopic analysis was performed by imaging the dried filters with a Keyence VHX−7000 digital microscope set to 150 × magnification (Pixel size: 4.058 μm). A Keyence OP−87429 polarisation illumination attachment was used to block reflective light and enhance contrast (Fig. 1b).

The MP extraction for surface analysis followed a similar procedure, with specific modifications to preserve particle integrity. To prevent artificial alterations to the surface, no harsh reagents such as $ZnCl_2$ or oxidative treatments were used [9,42]. Instead, deionised, pre-filtered water (MN QF−10, Macherey-Nagel) was used for density separation, as its density exceeds that of LLDPE (0.935 g cm^{-3}) [47]. For the PBAT/starch MPs, a potassium formate solution was applied again. After a 24-hour settling period, the supernatant was carefully transferred into Petri dishes using a glass pipette, rather than being filtered, and was subsequently dried at 40 °C in an oven (Fig. 1c). The recovered MPs were manually isolated under a digital microscope (Keyence VHX−7000) using stainless steel tweezers. The particles were then rinsed with deionised water and air-dried at room temperature (Fig. 1c).

To minimise airborne contamination, all work was conducted under a fume hood, with open beakers covered using aluminium foil. All laboratory equipment was plastic-free, consisting exclusively of metal or glass components, and rinsed with deionised water pre-filtered through a 0.2 μm glass fibre filter (MN QF−10, Macherey-Nagel) prior to use. Procedural blanks were prepared and analysed alongside every seventh sample, following identical processing steps. No black particles with morphological characteristics consistent with the target MPs were detected in any of the blanks, confirming negligible contamination throughout the analytical procedure.

Unspiked control plots were included at each field site and processed through the same workflow as the MP-spiked plots. Mean particle counts in control plots ranged from 20,480 to 56,400 MPs kg^{-1} soil across countries in 2022 and from 8340 to 18,273 MPs kg^{-1} soil in 2023.

2.4. Deep learning-based microplastic number and morphology analysis

2.4.1. Data

To automatically derive the number, as well as key morphological parameters of MP from the microscopic imagery, a deep learning model is employed. The experimental dataset for developing the deep microplastic detection model consists of microscopic RGB images X of prepared filters (Keyence VHX−7000, Magnification: 150 ×, Pixel size: 4.058 μm). These filters are partly manually annotated. The annotations Y provide masks which divide the images into the classes: *microplastic* (indicated by 1) and *background* (indicated by 0). To prepare the annotated data in a manner suitable for training a deep learning model, the annotated parts of the images are further subdivided into patches of size 256 × 256.

The patches are divided into training, validation, and test splits at the filter level. This is to ensure that testing is performed on filters not seen during training, such that the generalizability of the trained model can be assessed.

2.4.2. Model definition and training

Based on the training split of the dataset described above, a deep learning model F_θ is implemented using PyTorch [48] and trained to distinguish between MP and the background class:

$$\widehat{Y} = F_\theta(X)$$

where $\widehat{Y}$ contains the predicted probabilities of each pixel belonging to the MP class.

F_θ is implemented as a UNet [49] with a ResNet−18 backbone [50] using batch normalization [51], as implemented in the Segmentation Models Pytorch library [52]. The parameters of the model θ are optimized with respect to the binary cross-entropy loss $L(\widehat{Y}, Y)$ between the predicted and annotated MP masks:

$$L(\widehat{Y}, Y) = -\sum\nolimits_i [Y_i \log \widehat{Y}_i + (1 - Y_i)\log(1 - \widehat{Y})_i],$$

where the index i iterates over all image pixels and the corresponding predictions. For training, the Adam optimizer is used with a batch size of 32 and an initial learning rate of 5×10^{-4} [53]. The learning rate is linearly decreased throughout the training process until the final learning rate of 5×10^{-5} is reached. The model is trained for a maximum of 100 epochs with early stopping based on the validation dataset.

To improve the diversity of the training dataset, augmentation using random rotation and color jitter is used. For the latter, the brightness, contrast, saturation, and hue of the images are each modified by an individual multiplier, which is randomly sampled from 0.9 to 1.1. Additionally, to tackle the data imbalance in the dataset, patches that include MP are over-sampled by a factor of 20 compared to those only containing the background class.

To improve the robustness of the prediction and allow for assessing its uncertainty, model ensembling [54] is used by training $N = 5$ instances of the above-described model from different random initializations.

2.4.3. Model evaluation

To evaluate the model, the average of the probabilities predicted by the N ensemble members is used:

$$\hat{Y}^{(ens)} = \frac{1}{N}\sum_{i=0}^{N} \hat{Y}^{(i)},$$

where $\hat{Y}^{(i)}$ represents the prediction of the i-th ensemble member.

For evaluation, several quantitative metrics are used to quantify how well the ensembled predictions $\hat{Y}^{(ens)}$ match the annotations Y. To this end, the result is first represented as a binary mask by assigning each pixel of $\hat{Y}^{(ens)}$ with a predicted probability exceeding a threshold of $t = 0.5$ to the MP class and vice versa. Subsequently, the pixels are categorized into true positives (TP), true negatives (TN), false positives (FP), and false negatives (FN). These classifications are the basis for calculating the following metrics:

- Overall accuracy (Acc.) $(TP+TN)/(TP+TN+FP+FN)$ measures the ratio of correctly classified pixels.
- F1 score (F1) $(2TP)/(2TP+FP+FN)$ is the harmonic mean of precision and recall and provides a balanced quantification of how well the MP class is detected in particular.
- Intersection over Union (IoU) $(TP)/(TP+FP+FN)$ quantifies the spatial overlap between the predicted MP mask and the annotations.

All values range from 0% (complete disagreement) to 100% (perfect agreement). The final ensemble achieves an overall accuracy of 99.3%, an F1 score of 71.8%, and an IoU of 56.0% on the hold-out test set, indicating its overall ability to accurately classify MPs.

Several properties were derived from the predicted MP masks and the annotations and compared between the two. In addition to the number of MPs per filter, size and shape parameters of each MP were calculated. To determine the size, the area in pixels, the maximum Feret diameter, and the equivalent spherical diameter were calculated. The equivalent spherical diameter is the diameter of a sphere with the same volume as the plastic particle, whereas the maximum Feret diameter measures the length of the projected outline of the particle. For shape determination, the solidity was calculated, which is a measurement of the concavity of a particle [55]. It is a sensitive indicator of the roughness of particle edges and has been successfully used to distinguish between different MP morphologies, such as fragments, fibres and microspheres [56], with lower values indicating increasingly irregular particle edges [55]. This comparison provides a more interpretable and meaningful assessment of the model performance in the context of the task.

2.4.4. Model application and construction

To construct the final dataset, the trained model ensemble is applied to previously unconsidered images of samples. In addition to the averaged predictions, Fleiss' κ [57], a statistical measure for assessing the agreement between different ensemble members, is computed for each filter based on the averaged probabilities:

$$\kappa = \frac{P_0 - P_e}{1 - P_e},$$

where P_0 refers to the observed agreement between the ensemble members and P_e is the expected agreement of the ensemble members, i.e., the probability that they agree by chance. Thus, positive values close to 1 imply good agreement between the different ensemble members, values around 0 imply no agreement, while negative values imply systematic disagreement. Overall, κ serves as a measure for the reliability of the model ensemble and can be used to detect filters with possibly inaccurate predictions.

In particular, samples containing segmented filters with a Fleiss' κ score below 0.55 were excluded from the dataset. All segmented filters with a Fleiss' κ score below 0.8 were also checked manually for deviation from the actual RGB images and excluded if necessary; in total, seven samples were removed from the analysis. The supplementary information provides an example of a segmented filter (Figure S3; Supplementary Information). The final dataset (Table S1; Supplementary Information) contained 53 samples, 26 for LLDPE, and 27 for PBAT/starch. To confirm the identity of recovered particles, a representative subset of 118 LLDPE and 102 PBAT/starch MPs recovered from different field plots was analysed using Attenuated Total Reflectance-Fourier Transform Infrared Spectroscopy (Bruker LUMOS II FTIR microscope, Bruker Corporation, Billerica, United States), confirming all analysed particles to be the targeted polymers. The risk of false positives from visually similar soil particles was further minimised by the distinctive black colouration and shape of the spiked MPs and the selection of field sites with no prior history of mulch film use or biosolid application. Background contamination through other pathways cannot be entirely excluded, however.

2.5. Scanning electron microscopy

Four to six MPs from each sample group (e.g., PBAT/starch Spain 2022) and fraction, as well as original non-soil-exposed MPs, were mounted on conventional SEM pin stubs (Plano GmbH, Wetzlar, Germany) using either carbon tape or isopropanol (analytical grade); in the latter case, adhesion was driven solely by surface interactions. To ensure electrical conductivity, MPs were sputter-coated with a 10 nm Carbon layer using a Cressington Carbon Coater 108 carbon/A, equipped with a Cressington Thickness Monitor mtm10 (Cressington Coating Systems, Watford, England). SEM imaging was conducted using a ZEISS Auriga 60 (Carl Zeiss AG, Oberkochen, Germany) at 1 kV acceleration voltage and varying working distances of 1,9–4.2 mm. The particles were imaged with varying magnifications and pixel sizes from 2436 to 2.791 nm, resulting in imaged areas of 4.667×10^6 µm^2 (4.667 mm^2) for the largest pixel size and 6.113 µm^2 for the smallest pixel size, respectively. All imaging was carried out using a back-scattered electron (BSE) and secondary electron (SE) detector.

2.6. Data analysis

All statistical analyses were conducted in R version 4.5.1 [58] using RStudio version 2025.05.1 [59]. All figures were prepared with the *ggplot2* package [60].

2.6.1. Total number of microplastics and microplastic distribution in soil aggregates

The total number of LLDPE and PBAT/starch MPs (particles kg^{-1} soil) and their distribution between free and occluded soil fractions were analysed using a generalized linear mixed model (GLMM) and generalized linear model (GLM) in the *glmmTMB* package in R [61].

Total MP abundance was analysed using a GLMM with a negative binomial error distribution (nbinom2) and log link function to account for overdispersed count data. Polymer type, year, country, and the interaction between polymer type and year were included as fixed effects. A random intercept for *Sample_Group_Year* was included to account for repeated measurements within the same experimental plots (*Total_Number_kg* ~ *Country* + *Polymer* × *Year* + *(1|Sample_Group_Year)*).

The proportion of occluded particles was analysed using a beta-binomial GLMM with logit link. The number of occluded particles was modelled relative to the total number of particles per sample (occluded + free). The beta-binomial distribution was chosen to account for overdispersion in proportional count data arising from unobserved

heterogeneity among samples. Polymer type, year, country, and their interaction were included as fixed effects (*cbind(Occluded, Free)* ~ *Country* + *Polymer* × *Year*). As the variation in occlusion proportion was sufficiently captured by the beta-binomial error structure, no random effects were included in this model.

For both models, estimated marginal means (EMMs) were calculated using the *emmeans* package and back-transformed to the response scale to aid interpretation. Pairwise comparisons among EMMs were performed using Wald z-tests with Tukey adjustment for multiple comparisons. Statistical significance was assessed at $\alpha = 0.05$ [62].

Model assumptions and fit were evaluated using simulated residual diagnostics implemented in the *DHARMa* package. Residual tests indicated no deviation from uniformity, no remaining overdispersion, and no significant outliers [63].

Soil organic carbon (SOC), clay content, and water-stable aggregates were determined for each plot (Table S1; Supplementary Information). Multiple simple linear regression models were used to examine the effects of SOC, clay content, and water-stable aggregates on occluded particle distribution of LLDPE and PBAT/starch MPs [64].

2.6.2. Analysis of the size and shape of soil-exposed and original microplastic particles

Spearman's rank correlation analysis was used to assess the collinearity among size parameters (area, Feret diameter, and equivalent spherical diameter) [64].

To assess the morphological differences (Feret diameter, solidity) between soil-exposed MPs (MPs from 2022 and 2023) and the original, unexposed MPs, regression models were applied. These analyses served solely to confirm the existence of systematic differences between exposure groups (Original vs. 2022 vs. 2023); subsequent hierarchical models accounting for the full sampling structure are described in Section 2.6.3 and were used for inference.

The maximum Feret diameter was log-transformed prior to analysis to meet model assumptions and was analysed using a Gaussian GLM that included polymer type (LLDPE, PBAT/starch), exposure (original, 2022, 2023), and their interaction as predictors (log *(*Feret diameter) ~ Polymer × Exposure). Solidity was analysed using a beta regression model with a logit link function, fitted in the *glmmTMB* package [61]. The fixed effects included were polymer type, exposure, and their interaction. To account for heteroscedasticity between polymers and exposure groups, the dispersion parameter of the beta distribution was modelled as a function of polymer type and exposure status, which substantially improved model fit compared to a constant-dispersion model (*Solidity* ~ *Polymer* * *Exposure, dispformula* = ~ *Polymer* + *Exposure*).

Model performance was evaluated using marginal R^2 for the GLM and Ferrari's R^2 for the beta regression model, as implemented in the *performance* package [65]. Estimated marginal means and pairwise contrasts were computed using the *emmeans* package [62]. For the Feret diameter model, estimates were reported on the original scale following back-transformation from the logarithmic scale. For beta regression models, the results are reported on the response scale following back-transformation from the logit link. Multiple comparisons were adjusted using Tukey's method. Statistical significance was assessed at $\alpha = 0.05$.

Model diagnostics for both models were assessed using simulated residuals (*DHARMa* package) [63]. For the Feret diameter model, the dispersion test indicated adequate fit; residual uniformity and outlier tests were statistically significant. For the solidity model, the dispersion test indicated overdispersion, which was addressed by explicitly modelling dispersion heterogeneity as a function of polymer and fraction. Despite this correction, residual uniformity and outlier tests remained statistically significant. Given the exploratory nature of these preliminary models and the known sensitivity of the test results for large sample sizes (n = 200,783 particles), results are interpreted in terms of effect direction and magnitude rather than formal inference [63].

2.6.3. Analysis of the size and shape of microplastic particles exposed in different fractions, years and countries

To assess the differences in Feret diameter and solidity of MPs due to different conditions during soil exposure, e.g., fractions, years, and countries, two mixed-models were fitted.

Particle size was quantified using the maximum Feret diameter. Similar to the model in Section 2.6.2, the Feret diameter was log-transformed prior to modelling due to the right-skewed distribution. To examine the effects of polymer type, country, year, and particle fraction on particle size, a linear mixed-effects model (LMM) was fitted using the *lme4* package in R [66]. The model included Polymer (LLDPE, PBAT/starch), Fraction (free, occluded), Country (Finland, Germany, Spain), and Year (2022, 2023) as fixed effects, including the full factorial interaction between Polymer, Year, and Fraction. *Sample_Plot_Year* was included as a random intercept to account for particles originating from the same soil sample not being independent. Additionally, a random slope for Fraction within *Sample_Plot_Year* was included to permit variation in the effect of particle occlusion among samples (log *(*Feret diameter) ~ Polymer × Year × Fraction + Country + (1 + Fraction | Sample_Plot_Year)). Model parameters were estimated using restricted maximum likelihood (REML). The significance of the fixed effects was assessed using Satterthwaite's approximation for degrees of freedom, as implemented in the *lmerTest* package [67].

As solidity values ranged between 0 and 1, they were analysed using a beta generalized linear mixed-effects model fitted with the *glmmTMB* package, using a logit link function [61]. The same fixed and random effects structure as for the size model was used. Additionally, a dispersion model was specified to allow heterogeneity in variance as a function of Polymer and Fraction (*Solidity* ~ *Polymer* × *Year* × *Fraction* + *Country* + *(1* + *Fraction* | *Sample_Plot_Year, dispformula* = ~ *Polymer* + *Fraction*).

Model performance was evaluated using marginal and conditional R^2 as implemented in the *performance* package [65]. Estimated marginal means and pairwise contrasts were computed using the *emmeans* package and back-transformed to the response scale for interpretation [62]. As these hierarchical models of Feret diameter and solidity account for plot-level random effects and include the effects of fraction, year, and country, the resulting adjusted marginal means differed from those in Section 2.6.2.

Model assumptions were evaluated using simulation-based residual diagnostics implemented in the *DHARMa* package. For both the linear mixed-effects model (Feret diameter) and the beta mixed-effects model (solidity), simulated residual datasets were generated and inspected using quantile–quantile plots and residual versus fitted value plots [63]. The Feret diameter model showed no evidence of heteroscedasticity or model misspecification. Similar to Section 2.6.2, the dispersion test of the solidity indicated slight overdispersion, which was again addressed by explicitly modelling dispersion heterogeneity as a function of polymer and fraction. Tests for residual uniformity and outliers were statistically significant in both models. Due to large sample sizes (n = 176, 897 particles), model adequacy was therefore assessed based on visual inspection of residual diagnostics. The residual plots showed no evidence of model misspecification, non-linearity, or heteroscedasticity. Consequently, both models were considered suitable for making inferences [63].

3. Results

3.1. Incorporation of LLDPE and PBAT/starch MPs into soil aggregates across two years

The negative binomial GLMM revealed strong main effects of polymer type and year on total MP abundance, while no significant interaction between these factors was detected (Tables S2-S5; Supplementary Information). PBAT/starch MPs consistently showed a lower abundance than LLDPE MPs, and the abundance of both polymers declined markedly from 2022 to 2023. The abundance of LLDPE MPs decreased

significantly ($p < 0.001$) from 143,166 ± 19,500 MPs kg^{-1} soil to 57,988 ± 5790 MPs kg^{-1} soil, corresponding to a reduction of approximately 59%. A 52% reduction was observed for PBAT/starch, from 44,107 ± 7870 MPs kg^{-1} soil to 21,058 2850 MPs kg^{-1} soil (Fig. 2a and Figure S4; Supplementary Information). No effect of country was observed. The model showed high explanatory power (conditional $R^2 = 0.74$; marginal $R^2 = 0.72$) (Table S3; Supplementary Information). Observed particle numbers exceeded the control plots (20,480–56,400 MPs kg^{-1} soil in 2022 and 8340 - 18,273 MPs kg^{-1} soil in 2023), confirming that the majority of detected particles originated from the spiked MPs.

By contrast, the beta-binomial model only reflected a significant interaction between polymer type and year ($\beta = 0.99 \pm 0.38$ SE, $p < 0.01$), indicating that the proportion of occluded MPs changed differently over time for the two polymers (Tables S6−8; Supplementary Information). In 2022, the proportion of MPs in the occluded fraction was lower for PBAT/starch (43%) than for LLDPE (54%). By 2023, this pattern had reversed, with PBAT/starch showing a higher proportion of occluded MPs (76%) than LLDPE (65%) (Fig. 2b and Figure S4b; Supplementary Information). The increase for PBAT/starch (+33 %age points) was statistically significant ($p < 0.001$), while the change for LLDPE was modest and non-significant ($p = 0.32$). There were no statistically significant differences between polymer types within the same year. No country effect was detected.

Simple linear regression models revealed a significant positive relationship between clay content and the occluded fraction of LLDPE MPs in 2022 ($R^2 = 0.48$, $p = 0.008$) but not in 2023 ($p = 0.486$). No significant relationship between clay content and occluded PBAT/starch MPs was observed in either year. Neither water-stable aggregates nor SOC showed significant relationships with the occluded fraction for either polymer type or year (Figures S5−6; Supplementary Information).

3.2. Differences in the shape and size of the MPs – reference - exposed

Spearman's rank correlation analysis revealed significant correlations ($r = 0.97$, $p < 0.001$) between the Feret diameter and both the equivalent spherical diameter and the area of the MPs (Figure S7; Supplementary Information). Therefore, the Feret diameter was used for further analysis (other size parameters are shown in Figure S8; Supplementary Information).

Feret diameter and solidity differed significantly between soil-exposed (2022, 2023) and original particles, as well as between polymer types. These exploratory models were used to characterise the overall differences between soil-exposed and original MPs. The low explained variance for both models (Feret diameter: $R^2 = 0.037$; solidity: $R^2 = 0.035$) reflects the absence of random effects that account for

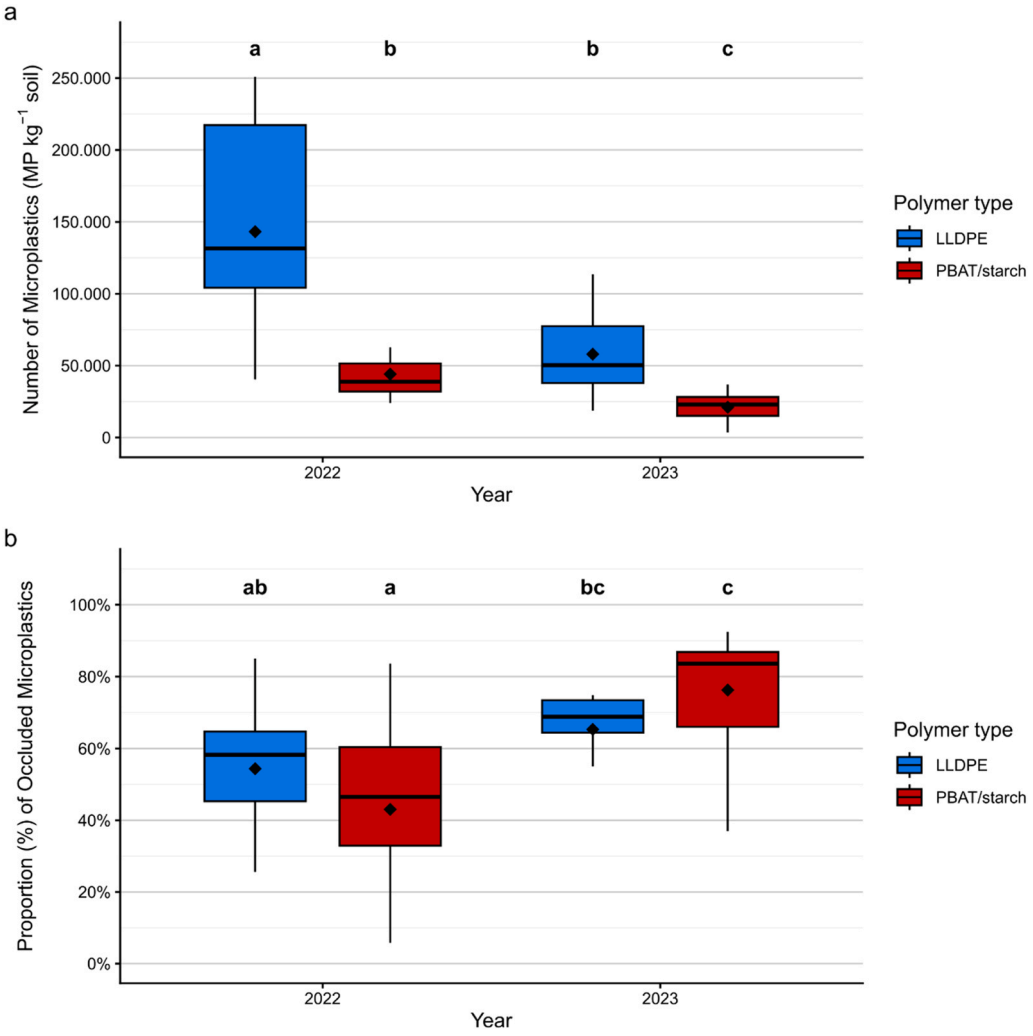

Fig. 2. (a) Total microplastic concentrations (free + occluded particles) (MP kg^{-1} soil) and (b) proportion of aggregate-occluded MPs for LLDPE and PBAT/starch MPs in 2022 and 2023. Diamonds indicate estimated marginal means (EMM), which were derived from (a) a negative binomial mixed model and (b) a beta binomial mixed model, respectively. Different letters indicate significant differences between groups based on Tukey-adjusted pairwise comparisons ($p < 0.05$). Boxes represent the interquartile range (IQR), horizontal lines the median, and whiskers extend to 1.5 × IQR.

clustering of MPs within the same sample plots and should be interpreted accordingly. Section 3.3 presents hierarchical models that incorporate the full experimental structure and yield improved model fit. The interaction between polymer type and exposure was significant for both morphological parameters ($p < 0.001$), indicating that the effect of soil exposure on particle morphology differed between LLDPE and PBAT/starch (Fig. 3 and Tables S9–15; Supplementary Information).

For the Feret diameter, divergent size trajectories were observed between polymer types. LLDPE MPs increased significantly in size from 2022 to 2023; however, they remained significantly smaller than the original MPs (all pairwise $p < 0.001$). In contrast, the size of the PBAT/starch MPs decreased significantly between 2022 and 2023, with the MPs being smaller in both years than the original MPs (all pairwise $p < 0.001$). In 2022, LLDPE MPs were significantly larger than PBAT/starch MPs (ratio = 1.09, $p < 0.001$), but this divergence became more pronounced by 2023, with LLDPE MPs being 1.65 times larger than PBAT/starch MPs ($p < 0.001$) (Tables S10–11; Supplementary Information).

Similarly, there were divergent temporal patterns of solidity between polymer types. The solidity of LLDPE MPs declined over time (2022: 0.850; 2023: 0.826) but was still significantly higher than that of the original LLDPE MPs (0.805; all pairwise $p < 0.001$). PBAT/starch MPs showed the opposite pattern, with solidity increasing slightly from 0.887 (2022) to 0.900 (2023). Meanwhile, the original PBAT/starch particles exhibited significantly lower solidity (0.879) than the exposed MPs ($p < 0.001$). Across all exposure conditions, the solidity of the PBAT/starch MPs was consistently higher than that of the LLDPE MPs (all pairwise $p < 0.001$) (Tables S14–15; Supplementary Information).

3.3. Differences in the shape and size of occluded and free microplastics

The linear mixed-effects model revealed a significant main effect of polymer type, fraction, and year on the Feret diameter. The significant interaction between polymer type and fraction ($p = 0.004$), indicated that the effect of occlusion differed between polymer types (Tables S16–17; Supplementary Information). Significant differences in size between the free (44.5 μm) and occluded (38.1 μm) LLDPE MPs were not observed ($p = 0.173$). In contrast, PBAT/starch particles were significantly larger in the occluded fraction (32.8 μm) than in the free

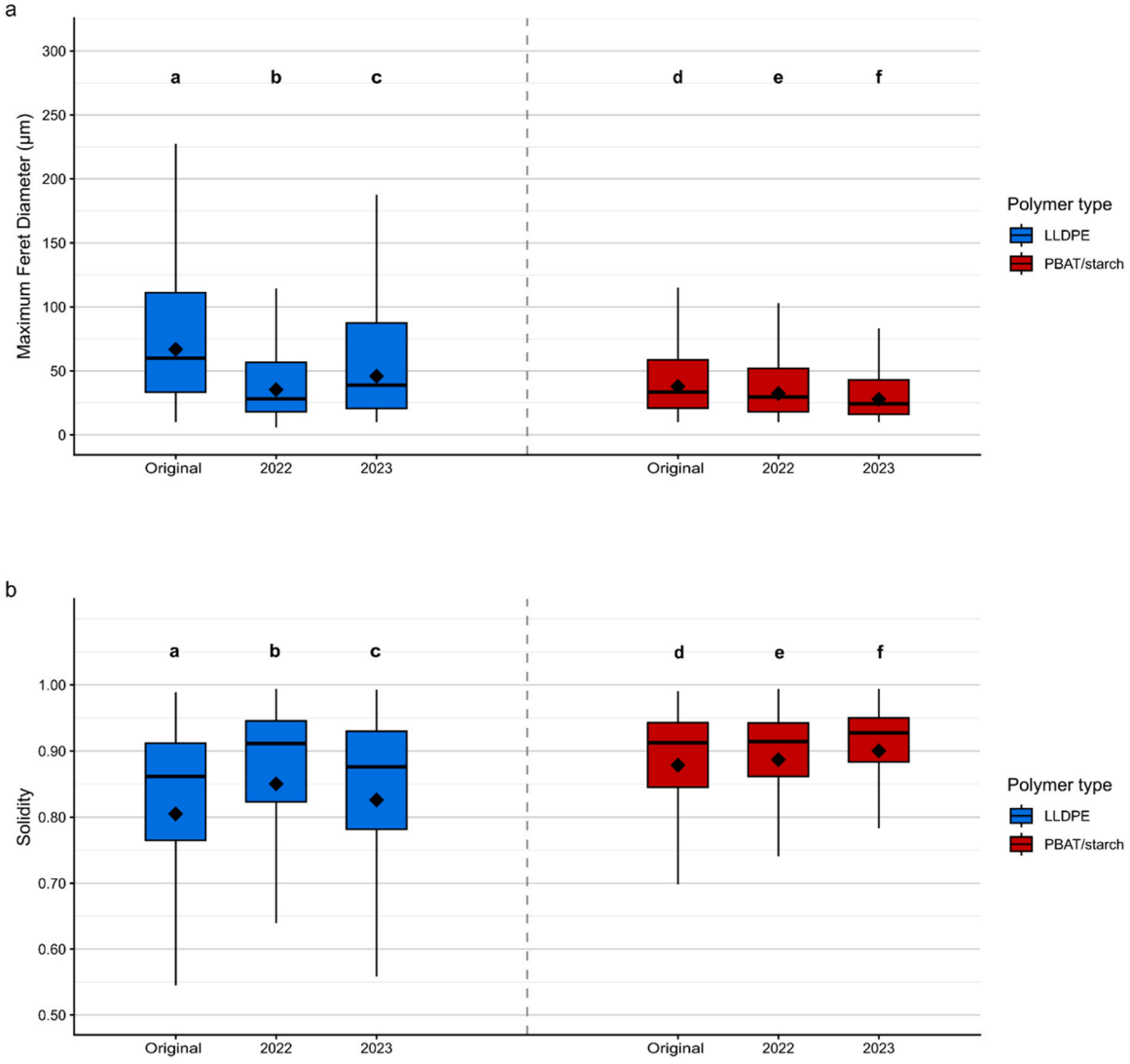

Fig. 3. (a) Maximum Feret diameter and (b) solidity of original LLDPE and PBAT/starch MPs, and soil-exposed MPs by polymer type and sampling year (2022 and 2023). Diamonds indicate estimated marginal means (EMM), which were derived from (a) a Gaussian generalized linear model and (b) a beta regression model. Different letters indicate significant differences between groups based on Tukey-adjusted pairwise comparisons ($p < 0.05$). Comparisons were conducted between original and soil-exposed MPs (combined from 2022 and 2023). For presentation purposes, the MPs from different years are separated. Boxes represent the interquartile range (IQR), horizontal lines the median, and whiskers extend to 1.5 × IQR.

fraction (23.7 μm; $p < 0.001$). Free LLDPE particles were 1.88 times larger than free PBAT/starch particles ($p < 0.001$), while in the occluded fraction, no significant difference between polymers was detected ($p = 0.139$) (Tables S18–19; Supplementary Information). Similarly, the interaction between polymer type and year was significant ($p < 0.001$), demonstrating that temporal changes in particle size depended on polymer type. LLDPE particles were significantly larger in 2023 (47.4 μm) than in 2022 (35.8 μm; $p < 0.001$), whereas PBAT/starch particles were significantly smaller in 2023 (24.7 μm) than in 2022 (31.5 μm; $p < 0.001$). In 2022, LLDPE and PBAT/starch did not differ significantly in size, whereas in 2023, a pronounced and significant difference was observed (Fig. 4a and Tables S20–21; Supplementary Information). Hence, the aggregate-associated dynamics of the MP interactions were polymer-specific. Yet, neither country nor the three-way interaction had a significant effect on particle size. Histograms showing the size distribution of LLDPE MPs revealed a selective loss of smaller particles (<100 μm) between 2022 and 2023, with larger particles being retained more effectively. By contrast, the size distribution of PBAT/starch MPs decreased proportionally across all size classes (Figure S9; Supplementary Information).

The GLMM model also revealed a significant main effect of polymer type, fraction, year, and country on the solidity of the MPs. Again, two significant interactions qualified these main effects. The significant interaction between polymer type and fraction ($p = 0.004$), reflected a difference in the effect of occlusion between polymer types (Fig. 4 and Tables S22–28; Supplementary Information). For LLDPE, occluded particles (0.863) were significantly more solid than free particles (0.807; $p < 0.001$). For PBAT/starch, the difference between fractions was much smaller (0.901 vs. 0.888) and only weakly significant ($p = 0.023$) (Tables S25–26; Supplementary Information). Again, also the interaction term between polymer × year was significant: LLDPE solidity declined significantly from 2022 (0.852) to 2023 (0.821; $p < 0.001$), whereas PBAT/starch solidity remained stable across years (0.891 vs. 0.899; $p = 0.178$). As both MP types exhibited seasonal changes in solidity, it seemed reasonable to assume that the differences in aggregate interactions between polymer types reflect variations in MP weathering rates, which then interact with aggregate turnover and reformation over different time scales. To better understand these processes, we therefore examined potential surface alteration processes in more detail using SEM.

3.4. Surface analysis using scanning electron microscopy

To assess the surface changes of the MPs during soil exposure, four to six MPs from each sample group and fraction were imaged and compared with the original, unexposed MPs. The original LLDPE MPs

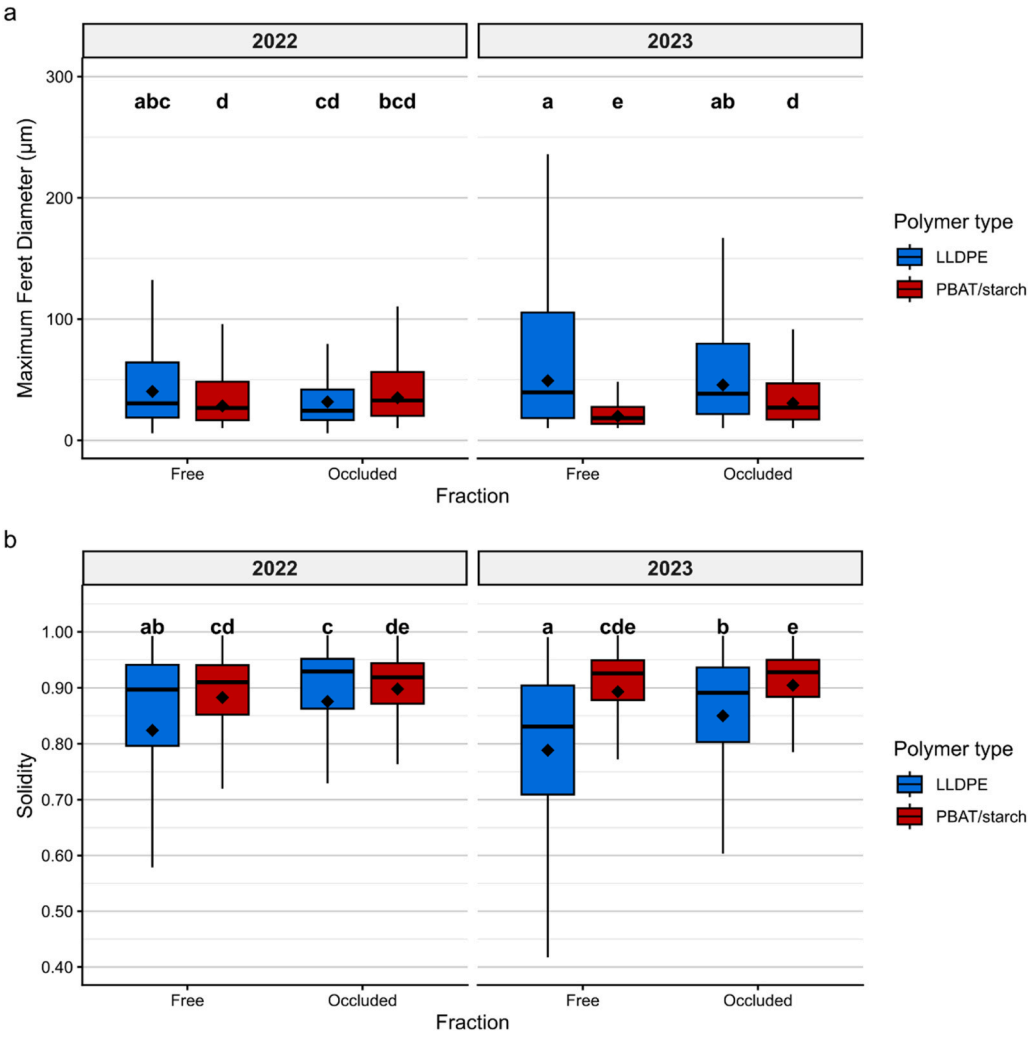

Fig. 4. (a) Maximum Feret diameter and (b) solidity of MPs in the free and occluded fractions for LLDPE and PBAT/starch MPs in 2022 and 2023. Diamonds indicate estimated marginal means (EMM), which were derived from (a) a linear mixed model and (b) a beta-distributed mixed model, respectively. Different letters indicate significant differences between groups based on Tukey-adjusted pairwise comparisons ($p < 0.05$). Boxes represent the interquartile range (IQR), horizontal lines the median, and whiskers extend to 1.5 × IQR.

were irregular in shape, often with several long, uneven filaments protruding from the main body (Figure S10a,b; Supplementary Information). The surface was uneven, though there were no deep cracks or holes (Fig. 5a and Figure S10b; Supplementary Information). Only a few surface adhesions and minor impurities were present (Fig. 5a). In contrast, the original PBAT/starch MPs had a more angular morphology and typically lacked filaments or had very short ones (Figure S11a; Supplementary Information). Their surface was noticeably rougher than that of the LLDPE MPs, featuring pits smaller than 1 μm that were distributed unevenly (Fig. 5b). In certain regions, net-like surface structures were present, which also contributed to the formation of small holes (Figure S11b; Supplementary Information).

Following exposure to soil, and regardless of aggregate occlusion, LLDPE MPs generally retained a morphology and surface structure similar to that of the original LLDPE. However, holes ranging from approximately 1 μm to 10 μm in diameter were observed to form in some particles after they had been in the soil for 6 months (Fig. 5c). At the edges, even holes smaller than 250 nm occurred. Additionally, small cracks around 5 μm in length developed and extended deep into the polymer matrix (Figures S10c-d; Supplementary Information). In images taken at lower magnification, larger cracks exceeding 30 μm in length were also visible (Figure S10e; Supplementary Information). No differences were observed between the 6- and 18-month-exposed MPs.

In contrast to LLDPE, the PBAT/starch MPs exhibited significantly greater surface roughness after exposure to soil, with scratches and cracks of various sizes developed on the MPs; some cracks even exceeded 100 μm in length (Figure S11c; Supplementary Information). Numerous holes were observed, ranging in diameter from 200 nm to over 5 μm (Fig. 5d and Figures S11c-f; Supplementary Information), with even smaller holes (0.2–1 μm) unevenly distributed across the entire surface.

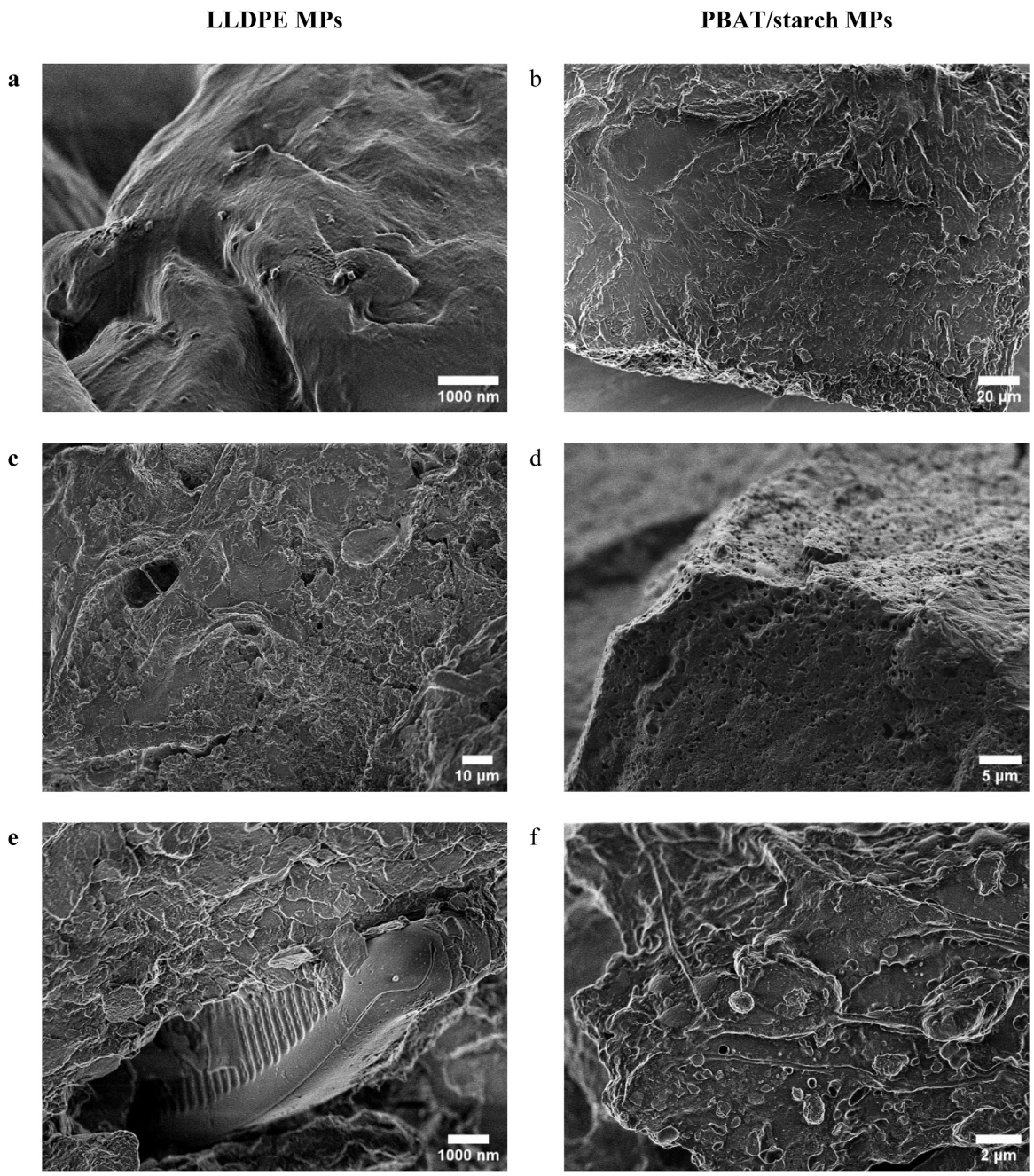

Fig. 5. Scanning electron microscopy (SEM) images of the surface of original (a) LLDPE and (b) PBAT/starch microplastics (MPs) and (c,d) MPs after soil exposure, with (e, f) attached microorganisms on the surface of MPs.

These surface features were already observed for MPs in all countries, regardless of an occlusion in aggregates or as free MPs, after the first sampling in 2022.

In addition to the formation of cracks and holes, both the LLDPE and the PBAT/starch MPs were covered with a thick surface coating that was clearly distinguishable from the underlying polymer. This dense layer consisted of pollen, algae, bacteria and mineral particles (Figures S10−11; Supplementary Information). In several instances, large cracks had also developed within this surface coating (Figure S10 g; Supplementary Information). In this coating, a variety of microorganisms were observed, with higher magnification images revealing individual organisms (Figures S10−11; Supplementary Information). Microbial colonisation patterns varied between sites, e.g., diatoms were found on an MP extracted from German soil only, but not found in the samples from the other countries (Fig. 5 and Figures S10−11; Supplementary Information). Although the surface structure obtained by SEM images showed a stronger alteration of the biodegradable polymers, it did not clearly indicate an effect of aggregate occlusion on MPs weathering.

4. Discussion

4.1. Fate of MPs in soil

The observed decline in LLDPE and PBAT/starch MP concentrations between 2022 and 2023 suggests that after soil application, the mulch-derived MP particles were not stable in the environment but have been lost by various processes. One potential mechanism is the vertical transport of MPs into deeper soil layers, facilitated by rainfall and infiltration [68,69] or through bioturbation, e.g., the activity of earthworms [28]. PBAT/starch MPs were consistently smaller than LLDPE MPs and were therefore more prone to downward transport, which may partly explain their particularly low concentrations after six months [27]. As soil sampling was restricted to the first 10 cm, such transported MPs would not have been detected. However, considering the recent findings reported by Rieckhof et al. [70], the low mobility observed in barley-cultivated soils suggests that infiltration and runoff are unlikely to be the primary mechanisms driving MP transport. Dilution by ploughing or other agricultural activities was likely minimal as the soils were managed using reduced tillage; i.e., the top 10 cm of soil was loosened, but not turned over. Therefore, lateral transport processes, such as wind-driven erosion, might redistribute MPs beyond the sampling area, thereby reducing the measured concentrations [71]. This may also explain the presence of MPs detected in unspiked control plots, which cannot be entirely excluded given the plot-based experimental design. This cross-contamination was probably further facilitated by the randomized block design of the field trial, as plots representing different treatments were located only a few meters apart, and may have occurred already during the implementation of the trial. Although climatic differences might influence the extent of such processes, there were no statistically significant differences observed between the countries.

In addition to physical transportation processes, the degradation and fragmentation of MPs likely contributed to the concentration decline, particularly for biodegradable PBAT/starch MPs [18]. Fragmentation of MPs may have produced smaller particles that then fell below the analytical detection limit of 10 µm (the pore size of the stainless-steel filters and exclusion criteria for the algorithm used). The consistently higher LLDPE concentrations across both years, at comparable initial concentrations at the start of the experiment, likely reflect its greater chemical stability compared to PBAT/starch [14]. Nevertheless, the loss of MPs between 2022 and 2023 was greater for LLDPE (59%) than for PBAT/starch (52%). We attribute this finding to changes in the incorporation into soil aggregates: the portion of MPs that was occluded within soil aggregates was lower for LLDPE in 2023 (65%) than for PBAT/starch (76%). Hence, there was a greater proportion of particles in the free fraction and, therefore, more susceptible to losses through transport processes [26]. In contrast, the higher occlusion of PBAT/-starch MPs (76%) may have partially protected them from such losses, despite their greater susceptibility to degradation and fragmentation [72].

This interpretation is supported by the finding that a significant proportion of MPs were occluded within soil aggregates, thus confirming our first hypothesis. The observed proportion of aggregate-occluded MPs in 2023–76% for PBAT/starch and 65% for LLDPE - is comparable to that reported by Zhang & Liu [7] for greenhouse soils in China, where approximately 72% of MPs were found within soil aggregates, but substantially higher than in other studies (28 and 35%, respectively) [71,73]. Aggregate occlusion increased for both polymers from 2022 to 2023. The increase in aggregate occlusion was statistically significant for PBAT/starch (+33 %age points, $p < 0.001$), but not for LLDPE (+11 %age points), confirming our second hypothesis that aggregate occlusion is polymer-specific. The concurrent decline in total MP abundance and increase in the proportion of occluded MPs further suggest that free MPs were lost at a higher rate than occluded MPs. This is consistent with findings for POM, which is physically protected by aggregate occlusion [31,74,75]. Similarly, occluded MPs seem to undergo preferential protection from degradation and transport due to reduced oxygen availability and limited microbial accessibility [73,76]. This pattern was particularly evident for PBAT/starch, where the absolute number of free particles decreased substantially while the occluded fraction increased.

The discrepancies between studies in the percentage of occluded MPs emphasise that the process of MP occlusion in soil aggregates is complex, and likely influenced by both MP properties, such as concentration, polymer type, size, and shape, as well as by soil properties, climatic conditions, and the time elapsed since entry into the soil [25,34,35,77]. A significant positive relationship between clay content and the occluded fraction of LLDPE MPs was observed in 2022, consistent with the well-established role of fine mineral particles in aggregate formation and stabilisation [33]. Yet, this relationship was not significant in 2023, and no equivalent relationship was found for PBAT/starch in either year. Similarly, a parallel study conducted within the same field experiment did not observe a systematic effect of the applied MPs on soil aggregate stability as assessed by water-stable aggregate content [41]. Nevertheless, disentangling individual effects from country-level differences in climate, soil properties, and biological activity was not possible within the present study design, which was also reflected in the substantial variation of occluded MPs between sites (Figures S4−5; Supporting Information). Together, these findings suggest that soil aggregates act as a significant long-term sink for MPs.

To comply with EU standards, biodegradable plastics must achieve at least 90% biodegradation within two years under controlled laboratory conditions (EN 17033:2018). However, under field conditions, biodegradable plastics often degrade much more slowly [72,78], and our data confirm that this rate may decrease further with soil aggregate occlusion, thus contributing to the persistence of biodegradable MPs in the environment. Conversely, occlusion also reduces the mobility, and hence the leaching, and immediate bioavailability of biodegradable MPs to plants and soil organisms, potentially mitigating ecotoxicity and short-term ecological impacts [79,80]. Disturbing the soil structure, e.g., through tillage operations, will lead to the immediate release of numerous occluded small MPs back into the soil matrix. This should, on the one hand, re-expose biodegradable MPs to aerobic conditions and microbial activity, thus potentially accelerating their mineralisation. On the other hand, the sudden release of occluded MPs back into the free fraction may account for sudden increases in MP bioavailability and ecotoxicity in the environment.

A limitation of the present study is that MPs of defined sizes were directly spiked into the soil rather than generated through the fragmentation of mulch films under field conditions. Under realistic agricultural conditions, biodegradable mulch films are typically tilled into the topsoil after their service life, producing residues ranging in size from macroplastics to small microplastics or even smaller, which

undergo progressive fragmentation in soil [6]. Conventional mulch films, in contrast, fragment primarily on the soil surface through abiotic weathering processes, generating predominantly small particles of different sizes, such as MPs, which may subsequently be incorporated into the topsoil [81]. Hence, the size distribution of the MPs used here might differ from the particle size spectrum found in mulch film-contaminated field soils [16,82]. As particle size influences both vertical transport and aggregate occlusion, the absolute occlusion rates and size-dependent patterns reported here may not be directly transferable to soils contaminated through natural mulch film degradation [26,83]. Nevertheless, the polymer-specific differences in occlusion dynamics and morphological changes observed in this study are expected to reflect fundamental material properties that are largely independent of the initial particle size distribution, and thus remain relevant for understanding the environmental fate of mulch film-derived MPs.

4.2. Properties of aggregate-occluded and free MPs

Soil exposure and weathering are known to affect MP properties such as size, solidity, and surface structure [9], which was confirmed by our results, even for the relatively short time period of 18 months. While soil-exposed MPs were significantly smaller than original MPs for both polymer types, the subsequent fate of the particles differed markedly between polymers. While LLDPE MPs showed an overall increase in Feret diameter during prolonged soil exposure, PBAT/starch particles became significantly smaller over time (Figs. 3 and 4). This opposite temporal trend indicates fundamentally different weathering and transport behaviours of the two polymers in soil.

The ongoing decrease in the size of PBAT/starch MPs suggests that biodegradable polymers are more susceptible to fragmentation and degradation [18,84], which was also reflected in the proportional decrease across all size classes observed in the size distribution histogram (Figure S9; Supporting Information). In contrast, the size increase of LLDPE MPs over time represents a selective loss of smaller particles through transport processes [27,85], as evidenced by the preferential loss of particles below 100 μm in the size distribution histogram, leading to a relative enrichment of larger particles in the sampled soil (Figure S9; Supporting Information). Additionally, the accumulation of soil minerals and microorganisms on the surface of MPs, as imaged by SEM (Fig. 5), may have contributed to a lesser extent to the observed increase in particle size.

Different weathering or stabilization processes were also indicated by the polymer-specific pattern observed for the occlusion in soil aggregates. For LLDPE, larger particles were predominantly found in the free fraction, whereas for PBAT/starch, larger particles were associated with the occluded fraction. For PBAT/starch, occlusion in aggregates hampers microbial and enzyme accessibility or oxygen availability, thereby slowing degradation and fragmentation. This stabilization mechanism is well known for POM, where organic material is preferentially preserved within soil aggregates [31]. First indications of such behaviour for biodegradable plastics were reported by Zhang et al. [73], who observed reduced degradation and fragmentation rates of polylactic acid/PBAT blends associated with soil aggregates. For LLDPE, aggregate incorporation might be size-selective [83], as larger MPs may be less likely to be incorporated into aggregates and thus remain predominantly in the soil matrix. The relative enrichment of large particles in the free phase may have contributed to the observed pattern.

As was already apparent in the original materials, PBAT/starch MPs consistently exhibited higher solidity values than LLDPE MPs. This baseline discrepancy can be attributed to differences in particle morphology. Overview-SEM images showed that PBAT/starch MPs were more angular, whereas LLDPE MPs had filamentous protrusions extending from their bodies (Figures S10–11, Supporting Information). These protrusions are probably caused by the greater elongation at break of LLDPE, which leads to stretching of the material and formation of filaments during cryomilling [40]. Such filaments increase edge irregularity and thus reduce solidity independently of soil exposure.

The solidity of soil-exposed MPs showed distinctive changes over time and between fractions, likely reflecting two confounding processes. First, ongoing weathering in soil altered MP solidity in a polymer-specific manner: The solidity of LLDPE decreased significantly from 2022 to 2023, likely reflecting increased surface irregularity due to weathering processes [9], whereas the solidity of PBAT/starch MPs increased slightly, consistent with surface erosion as the predominant biodegradation mechanism [84]. When material is preferentially lost from the surface of a particle, its edges become progressively smoother while its overall shape is retained [84] - an interpretation that is further supported by the concurrent decrease in the size of PBAT/starch MPs. These trends contrast with the pronounced long-term increase in solidity (from 0.65 to 0.78) reported by Bai et al. [15] for soil-derived MPs under mulch application for over 30 years. Deviating trends might be attributed to the much shorter observation period of the present study (18 months) and the higher initial solidity of the well-defined MPs used here.

Second, occluded MPs were significantly more solid than free MPs for both polymers, which may reflect preferential incorporation of smoother, more regularly shaped MPs into soil aggregates, rather than occlusion solely protecting MPs from weathering [73]. More solid particles may interact more effectively with mineral surfaces and organic matter, making them more likely to become occluded. Especially for PBAT/starch, this interpretation fits the observed pattern in which ongoing weathering progressively increased solidity over time, potentially enhancing their affinity for mineral surfaces and thereby increasing their likelihood of occlusion. However, no clear differences could be distinguished between fractions or years using SEM imaging, likely reflecting a complex interaction of both processes, whereby more weathered MPs may be more prone to occlusion, while occlusion itself protects MPs from further weathering. To disentangle these processes, more detailed and fraction-specific analyses using additional techniques are necessary in future studies.

5. Conclusion

The results demonstrate that both conventional LLDPE and biodegradable PBAT/starch MPs are substantially incorporated into soil aggregates, with occlusion increasing over time. Aggregate occlusion is polymer-specific, with a more pronounced increase for PBAT/starch, reflecting differential interactions between MP types and soil aggregates. Soil exposure altered the morphological properties of both polymer types, with changes in size and shape indicating ongoing weathering over the observation period. The interaction between polymer type and aggregate occlusion further suggests that MP weathering and soil aggregate dynamics are coupled, with polymer-specific alterations influencing the extent and trajectory of aggregate incorporation. Together, these findings confirm that soil aggregate occlusion is a key mechanism governing the fate and residence time of MPs in agricultural soils. The kinetics of aggregate formation and breakdown, and how these processes interact with the weathering of different MP types, warrant further investigation.

Environmental Implication

Information on the incorporation of MPs into soil aggregates under field conditions remains limited. This study demonstrates that, regardless of polymer type, MPs become increasingly occluded within soil aggregates over time, indicating that soil aggregation is an important mechanism for retaining MPs in agricultural soils. While the occlusion of MPs may reduce their mobility and short-term bioavailability, it simultaneously enhances their persistence by shielding particles from environmental degradation processes. This is particularly relevant for biodegradable plastics: although PBAT/starch particles exhibited significant surface changes, their incorporation into soil aggregates may

impede complete degradation under field conditions. Overall, these findings emphasise the need to consider soil structure and aggregation processes when assessing the long-term persistence and environmental risks of conventional and biodegradable MPs in soils.

CRediT authorship contribution statement

Helena Soinne: Writing – original draft, Funding acquisition. **Rafaela Debastiani:** Writing – original draft, Funding acquisition. **Salla Selonen:** Writing – original draft, Funding acquisition. **Christina Bogner:** Writing – original draft. **Vera Schlierenkamp:** Investigation. **Johannes Leonhardt:** Writing – original draft, Investigation. **Torsten Scherer:** Writing – original draft, Funding acquisition. **Melanie Braun:** Writing – original draft, Funding acquisition, Conceptualization. **Virtudes Martínez-Hernández:** Writing – original draft, Funding acquisition. **Matthias Mail:** Writing – original draft. **Rachel Hurley:** Writing – original draft, Funding acquisition. **Wulf Amelung:** Writing – original draft, Funding acquisition, Conceptualization. **Larissa Hennig:** Investigation. **Redondo-Hasselerharm Paula:** Writing – original draft, Funding acquisition. **Max Groß:** Writing – original draft, Investigation, Conceptualization. **Ribana Roscher:** Writing – original draft, Conceptualization. **Luca Nizzetto:** Writing – review & editing, Funding acquisition.

Declaration of Generative AI and AI-assisted technologies in the writing process

During the preparation of this work the authors used Claude Sonnet 4.6 (Anthropic) and DeepL Write (Deepl SE) to enhance readability and clarity. After using this tools/services, the authors reviewed and edited the content as needed and take full responsibility for the content of the publication.

Declaration of Competing Interest

The authors declare that they have no known competing financial interests or personal relationships that could have appeared to influence the work reported in this paper.

Acknowledgements

This work was funded by the European Union's Horizon 2020 - Research and Innovation Framework Programme PAPILLONS (grant agreement no 101000210) and the European Research Council (ERC Starting Grant NanoSoil; grant no 101163487). In addition, W. Amelung, M. Braun, and R. Roscher acknowledge additional support from the Deutsche Forschungsgemeinschaft (DFG, German Research Foundation) under Germany's Excellence Strategy, EXC2070 – 390732324 - PhenoRob. C. Bogner acknowledges the funding by the Deutsche Forschungsgemeinschaft (DFG, German Research Foundation) – Project Number 391977956 SFB 1357. J. Leohnardt acknowledges the funding of Deutsche Forschungsgemeinschaft (DFG, German Research Foundation) – Project Number: 450058266 SFB 1502/1–2022. This work was partly carried out with the support of the Karlsruhe Nano Micro Facility (KNMFi, www.knmf.kit.edu), a Helmholtz Research Infrastructure at Karlsruhe Institute of Technology (KIT, www.kit.edu).

Appendix A. Supporting information

Supplementary data associated with this article can be found in the online version at doi:10.1016/j.jhazmat.2026.143175.

Data availability

Data will be made available on request.

References

[1] Kedzierski, M., Cirederf-Boulant, D., Palazot, M., Yvin, M., Bruzaud, S., 2023. Continents of plastics: an estimate of the stock of microplastics in agricultural soils. Sci Total Environ 880, 163294.
[2] Kumar, R., Singh, V.P., 2022. Plasticulture engineering and technology. CRC Press, Boca Raton.
[3] Astner, A.F., Gillmore, A.B., Yu, Y., Flury, M., DeBruyn, J.M., Schaeffer, S.M., Hayes, D.G., 2023. Formation, behavior, properties and impact of micro- and nanoplastics on agricultural soil ecosystems (a review). NanoImpact 31, 100474.
[4] Bläsing, M., Amelung, W., 2018. Plastics in soil: analytical methods and possible sources. Sci Total Environ 612, 422–435.
[5] Demo, A.H., Asefa Bogale, G., 2024. Enhancing crop yield and conserving soil moisture through mulching practices in dryland agriculture. Front Agron 6.
[6] Kasirajan, S., Ngouajio, M., 2012. Polyethylene and biodegradable mulches for agricultural applications: a review. Agron Sustain Dev 32, 501–529.
[7] Zhang, G.S., Liu, Y.F., 2018. The distribution of microplastics in soil aggregate fractions in southwestern China. Sci Total Environ 642, 12–20.
[8] Kapanen, A., Schettini, E., Vox, G., Itävaara, M., 2008. Performance and Environmental Impact of Biodegradable Films in Agriculture: a Field Study on Protected Cultivation. J Polym Environ 16, 109–122.
[9] Groß, M., Mail, M., Debastiani, R., Scherer, T., Braun, M., 2025. Weathering of plastics in terrestrial environments. TRAC-Trend Anal Chem 190, 118281.
[10] Baby, M.G., Gerritse, J., Beltran-Sanahuja, A., Wolter, H., Rohais, S., Romero-Sarmiento, M.-F., 2025. Aging of plastics and microplastics in the environment: a review on influencing factors, quantification methods, challenges, and future perspectives. Environ Sci Pollut Res 32, 1009–1042.
[11] Gewert, B., Plassmann, M.M., MacLeod, M., 2015. Pathways for degradation of plastic polymers floating in the marine environment. Environ Sci Process & Impacts 17, 1513–1521.
[12] Feldman, D., 2002. Polymer Weathering: Photo-Oxidation. J Polym Environ 10, 163–173.
[13] Maqbool, A., Guzmán, G., Fiener, P., Wilken, F., Soriano, M.-A., Gómez, J.A., 2024. Tracing macroplastics redistribution and fragmentation by tillage translocation. J Hazard Mater 477, 135318.
[14] Arutchelvi, J., Sudhakar, M., Arkatkar, A., Doble, M., Bhaduri, S., Uppara, P.V., 2008. Biodegradation of polyethylene and polypropylene. Indian J Biotechnol 7.
[15] Bai, R., Liu, H., Cui, J., Wu, Y., Guo, X., Liu, Q., Liu, Q., Gao, H., Yan, C., He, W., 2024. The characteristics and influencing factors of farmland soil microplastic in Hetao Irrigation District, China. J Hazard Mater 465, 133472.
[16] Cao, J., Gao, X., Hu, Q., Li, C., Song, X., Cai, Y., Siddique, K.H., Zhao, X., 2023. Distribution characteristics and correlation of macro- and microplastics under long-term plastic mulching in northwest China. Soil Tillage Res 231, 105738.
[17] Menossi, M., Cisneros, M., Alvarez, V.A., Casalongué, C., 2021. Current and emerging biodegradable mulch films based on polysaccharide bio-composites. A review. Agron Sustain Dev 41.
[18] Campanale, C., Galafassi, S., Di Pippo, F., Pojar, I., Massarelli, C., Uricchio, V.F., 2024. A critical review of biodegradable plastic mulch films in agriculture: Definitions, scientific background and potential impacts. TRAC-Trend Anal Chem 170, 117391.
[19] Bastioli, C., 2020. Handbook of Biodegradable Polymers. De Gruyter.
[20] Itabana, B.E., Mohanty, A.K., Dick, P., Sain, M., Bali, A., Tiessen, M., Lim, L.-T., Misra, M., 2024. Poly (Butylene Adipate-Co-Terephthalate) (PBAT) – Based Biocomposites: A Comprehensive Review. Macro Mater & Eng 309.
[21] Akhir, M.A.M., Zubir, S.A., Mariatti, J., 2023. Effect of different starch contents on physical, morphological, mechanical, barrier, and biodegradation properties of tapioca starch and poly(butylene adipate-co-terephthalate) blend film. Polym Advan Technol 34, 717–730.
[22] Qin, M., Chen, C., Song, B., Shen, M., Cao, W., Yang, H., Zeng, G., Gong, J., 2021. A review of biodegradable plastics to biodegradable microplastics: another ecological threat to soil environments? J Clean Prod 312, 127816.
[23] Chinaglia, S., Esposito, E., Tosin, M., Pecchiari, M., Degli Innocenti, F., 2024. Biodegradation of plastics in soil: the effect of water content. Polym Degrad Stabil 222, 110691.
[24] Pischedda, A., Tosin, M., Degli-Innocenti, F., 2019. Biodegradation of plastics in soil: the effect of temperature. Polym Degrad Stabil 170, 109017.
[25] Kim, M.S., Chang, H., Zheng, L., Yan, Q., Pfleger, B.F., Klier, J., Nelson, K., Majumder, E.L.-W., Huber, G.W., 2023. A review of biodegradable plastics: chemistry, applications, properties, and future research needs. Chem Rev 123, 9915–9939.
[26] Rehm, R., Zeyer, T., Schmidt, A., Fiener, P., 2021. Soil erosion as transport pathway of microplastic from agriculture soils to aquatic ecosystems. Sci Total Environ 795, 148774.
[27] Connor, D.O., Pan, S., Shen, Z., Song, Y., Jin, Y., Wu, W.-M., Hou, D., 2019. Microplastics undergo accelerated vertical migration in sand soil due to small size and wet-dry cycles. Environ Pollut (Barking Essex 1987) 249, 527–534.
[28] Rillig, M.C., Ziersch, L., Hempel, S., 2017. Microplastic transport in soil by earthworms. Sci Rep 7, 1362.
[29] Six, J., Paustian, K., Elliott, E.T., Combrink, C., 2000. Soil structure and organic matter I. Distribution of aggregate-size classes and aggregate-associated carbon. Soil Sci Soc Am J 64, 681–689.
[30] Tisdall, J.M., Oades, J.M., 1982. Organic matter and water-stable aggregates in soils. J Soil Sci 33, 141–163.
[31] Golchin, A., Oades, J.M., Skjemstad, J.O., Clarke, P., 1994. Soil structure and carbon cycling. Aust J Soil Res 32, 1043–1068.

[32] Liu, B., Shen, Z., Zhou, Q., Hu, L., Zeng, G., Wang, X., Zhang, M., Zhang, D., Pan, X., 2024. Microplastics in soil aggregates: analytical methods, occurrence patterns, impact analyses and removal approaches, TRAC-Trend. Anal Chem 178, 117855.
[33] Totsche, K.U., Amelung, W., Gerzabek, M.H., Guggenberger, G., Klumpp, E., Knief, C., Lehndorff, E., Mikutta, R., Peth, S., Prechtel, A., Ray, N., Kögel-Knabner, I., 2018. Microaggregates in soils. J Plant Nutr Soil Sci 181, 104–136.
[34] Lehmann, A., Leifheit, E.F., Gerdawischke, M., Rillig, M.C., 2021. Microplastics have shape- and polymer-dependent effects on soil aggregation and organic matter loss – an experimental and meta-analytical approach. Micro &Nanopl 1.
[35] Lozano, Y.M., Lehnert, T., Linck, L.T., Lehmann, A., Rillig, M.C., 2021. Microplastic shape, polymer type, and concentration affect soil properties and plant biomass. Front Plant Sci 12, 616645.
[36] Zhang, H., Huang, Y., An, S., Zhao, J., Xiao, L., Li, H., Huang, Q., 2022. Microplastics trapped in soil aggregates of different land-use types: a case study of Loess Plateau terraces, China. Environ Pollut (Barking Essex 1987) 310, 119880.
[37] Golchin, A., Oades, J.M., Skjemstad, J.O., Clarke, P., 1994. Study of free and occluded particulate organic matter in soils by solid state 13C Cp/MAS NMR spectroscopy and scanning electron microscopy. Aust J Soil Res 32, 285–309.
[38] Lavallee, J.M., Soong, J.L., Cotrufo, M.F., 2020. Conceptualizing soil organic matter into particulate and mineral-associated forms to address global change in the 21st century. Glob Chang Biol 26, 261–273.
[39] John, B., Yamashita, T., Ludwig, B., Flessa, H., 2005. Storage of organic carbon in aggregate and density fractions of silty soils under different types of land use. Geoderma 128, 63–79.
[40] Hurley, R., Binda, G., Briassoulis, D., Carroccio, S.C., Cerruti, P., Convertino, F., Dvořáková, D., Kernchen, S., Laforsch, C., Löder, M.G.L., Pulkrabova, J., Schettini, E., Spanu, D., Tsagkaris, A.S., Vox, G., Nizzetto, L., 2024. Production and characterisation of environmentally relevant microplastic test materials derived from agricultural plastics. Sci Total Environ 946, 174325.
[41] Šmídová, K., Soinne, H., Kim, S.W., Tirronniemi, J., Meffe, R., Redondo-Hasselerharm, P.E., Braun, M., Rillig, M.C., Fritze, H., Adamczyk, B., Nikama, J., Kaseva, J., Saartama, V., Amelung, W., Hurley, R., Hofman, J., Nizzetto, L., Selonen, S., Velmala, S., 2025. Conventional and biodegradable agricultural microplastics: effects on soil properties and microbial functions across a European pedoclimatic gradient. Environ Pollut (Barking Essex 1987) 386, 127212.
[42] Peneva, S., Le, Q.N.P., Munhoz, D.R., Wrigley, O., Wille, F., Doose, H., Halsall, C., Harkes, P., Sander, M., Braun, M., Amelung, W., 2024. Microplastic analysis in soils: a comparative assessment. Ecotoxicol Environ Saf 289, 117428.
[43] Thomas, D., Schütze, B., Heinze, W.M., Steinmetz, Z., 2020. Sample preparation techniques for the analysis of microplastics in soil—a review. Sustainability 12, 9074.
[44] Jarosz, K., Natkański, P., Michalik, M., 2022. Microplastic extraction from the sediment using potassium formate water solution (H2O/KCOOH). Minerals 12, 269.
[45] Hurley, R.R., Lusher, A.L., Olsen, M., Nizzetto, L., 2018. Validation of a method for extracting microplastics from complex, organic-rich, environmental matrices. Environ Sci Technol 52, 7409–7417.
[46] Möller, J.N., Heisel, I., Satzger, A., Vizsolyi, E.C., Oster, S.D.J., Agarwal, S., Laforsch, C., Löder, M.G.J., 2022. Tackling the challenge of extracting microplastics from soils: a protocol to purify soil samples for spectroscopic analysis. Environ Toxicol Chem 41, 844–857.
[47] Osswald M., Baur E., Brinkmann S., Oberbach K., Schmachtenberg E. 2006. Int Plast Handb Resour Plast Eng 4th Ed Hanser Munich.
[48] Paszke, A., Gross, S., Massa, F., Lerer, A., Bradbury, J., Chanan, G., Killeen, T., Lin, Z., Gimelshein, N., Antiga, L., Desmaison, A., Kopf, A., Yang, E., DeVito, Z., Raison, M., Tejani, A., Chilamkurthy, S., Steiner, B., Fang, L., Bai, J., Chintala, S., 2019. PyTorch: an imperative style, high-performance deep learning library. In: Wallach, H., Larochelle, H., Beygelzimer, A., d\textquotesingle Alché-Buc, F., Fox, E., Garnett, R. (Eds.), Advances in Neural Information Processing Systems. Curran Associates, Inc.
[49] Ronneberger, O., Fischer, P., Brox, T., 2015. U-Net: convolutional networks for biomedical image segmentation. In: Navab, N., Hornegger, J., Wells, W.M., Frangi, A.F. (Eds.), Medical Image Computing and Computer-Assisted Intervention – MICCAI 2015. Springer International Publishing, Cham, pp. 234–241.
[50] He, K., Zhang, X., Ren, S., Sun, J., 2016. Deep residual learning for image recognition. In: 2016 IEEE Conference on Computer Vision and Pattern Recognition (CVPR). IEEE, pp. 770–778.
[51] S. Ioffe, C. Szegedy, Batch Normalization: Accelerating Deep Network Training by Reducing Internal Covariate Shift, arXiv, 2015.
[52] Iakubovskii, P., 2019. Segmentation Models Pytorch. GitHub.
[53] D.P. Kingma, J. Ba, Adam: A Method for Stochastic Optimization, arXiv, 2014.
[54] Lakshminarayanan, B., Pritzel, A., Blundell, C., 2017. Simple and scalable predictive uncertainty estimation using deep ensembles. In: Guyon, I., Von Luxburg, U., Bengio, S., Wallach, H., Fergus, R., Vishwanathan, S., Garnett, R. (Eds.), Advances in Neural Information Processing Systems. Curran Associates, Inc.
[55] Schnepf, U., von Moers-Meßmer, M.A.L., Brümmer, F., 2023. A practical primer for image-based particle measurements in microplastic research. Micro &Nanopl 3.
[56] Long, B.B., Li, F.Y., Wang, K., Huang, Y.Z., Yang, Y.J., Xie, D., 2023. Impact of plastic film mulching on microplastic in farmland soils in Guangdong province, China. HELIYON 9.
[57] Fleiss, J.L., Cohen, J., 1973. The equivalence of weighted kappa and the intraclass correlation coefficient as measures of reliability. Educ Psychol Meas 33, 613–619.
[58] R Core Team, R: A Language and Environment for Statistical Computing, R Foundation for Statistical Computing, Vienna, Austria, 2025.
[59] team, Posit, 2025. RStudio: integrated development environment for R., posit software. PBC, Boston, MA.
[60] Wickham, H., 2016. ggplot2: elegant graphics for data analysis. Springer, Switzerland.
[61] McGillycuddy, M., Warton, D.I., Popovic, G., Bolker, B.M., 2025. Parsimoniously fitting large multivariate random effects in glmmTMB. J Stat Soft 112.
[62] Lenth R., Piaskowski J. 2025. emmeans Estim Marg Means aka Least-Sq Means.
[63] Hartig F. 2024. DHARMa residual Diagn hierarchical (multi-Lev/mixed) Regres Models.
[64] Kassambara A. 2025. ggpubr 'ggplot2' Based Publ Ready Plots.
[65] Lüdecke, D., Ben-Shachar, M., Patil, I., Waggoner, P., Makowski, D., 2021. performance: an R package for assessment, comparison and testing of statistical models. JOSS 6, 3139.
[66] Bates, D., Mächler, M., Bolker, B., Walker, S., 2015. Fitting linear mixed-effects models using lme4. J Stat Soft 67.
[67] Kuznetsova, A., Brockhoff, P.B., Christensen, R.H.B., 2017. lmerTest package: tests in linear mixed effects models. J Stat Soft 82.
[68] Yu, H., Zhang, W., Li, J., Yang, J., Yang, X., Hai, C., Wang, Y., Yang, Y., 2025. Vertical distribution and multi-source pathways of microplastics in agricultural soils: a study of typical irrigation areas in the upper Yellow River basin. Environ Pollut (Barking Essex 1987) 381, 126479.
[69] Zhang, X., Liu, Y., He, D., 2025. Earthworms multifacetedly drive size- and type-dependent microplastic transport in soils. Environ Pollut (Barking Essex 1987) 382, 126789.
[70] Rieckhof, C., Martínez-Hernández, V., Tirroniemi, J., Sillanpää, M., Dvorakova, D., Tsagkaris, A.S., González-Ubierna, S., Hurley, R., Nizzetto, L., Rico, A., Meffe, R., 2026. Tracking biodegradable microplastics: Mobility in agricultural soils under different environmental conditions. J Hazard Mater 510, 142177.
[71] Yang, M., Tian, X., Guo, Z., Chang, C., Li, J., Guo, Z., Li, H., Liu, R., Wang, R., Li, Q., Zou, X., 2022. Effect of dry soil aggregate size on microplastic distribution and its implications for microplastic emissions induced by wind erosion. Environ Sci Technol Lett 9, 618–624.
[72] Coutris, C., Rivier, P.-A., Torp, T., Klaus, J., Joner, E.J., 2025. situ degradation of biodegradable plastic mulch in Nordic agricultural soils. Chemosphere 384, 144516.
[73] Zhang, M., Wang, L., Hou, L., Li, C., 2025. Novel insight into the in-situ study of biodegradable microplastics in soil aggregates. J Hazard Mater 497, 139692.
[74] Six, J., Bossuyt, H., Degryze, S., Denef, K., 2004. A history of research on the link between (micro)aggregates, soil biota, and soil organic matter dynamics. Soil Tillage Res 79, 7–31.
[75] Amelung, W., Zech, W., 1996. Organic species in ped surface and core fractions along a climosequence in the prairie, North America. Geoderma 74, 193–206.
[76] Ebrahimi, A., Or, D., 2015. Hydration and diffusion processes shape microbial community organization and function in model soil aggregates. Water Resour Res 51, 9804–9827.
[77] Fang, Z., Sallach, J.B., Hodson, M.E., 2024. Size- and concentration-dependent effects of microplastics on soil aggregate formation and properties. J Hazard Mater 465, 133395.
[78] Sintim, H.Y., Bary, A.I., Hayes, D.G., Wadsworth, L.C., Anunciado, M.B., English, M.E., Bandopadhyay, S., Schaeffer, S.M., DeBruyn, J.M., Miles, C.A., Reganold, J.P., Flury, M., 2020. situ degradation of biodegradable plastic mulch films in compost and agricultural soils. Sci Total Environ 727, 138668.
[79] Adamczyk, S., Zantis, L.J., van Loon, S., van Gestel, C.A.M., Bosker, T., Hurley, R., Nizzetto, L., Adamczyk, B., Velmala, S., 2024. Biodegradable microplastics induce profound changes in lettuce (Lactuca sativa) defense mechanisms and to some extent deteriorate growth traits. Environ Pollut (Barking Essex 1987) 363, 125307.
[80] Zantis, L.J., Adamczyk, S., Velmala, S.M., Adamczyk, B., Vijver, M.G., Peijnenburg, W., Bosker, T., 2024. Comparing the impact of microplastics derived from a biodegradable and a conventional plastic mulch on plant performance. Sci Total Environ 935, 173265.
[81] Steinmetz, Z., Schröder, H., 2022. Plastic debris in plastic-mulched soil-a screening study from western Germany. PEERJ 10, e13781.
[82] Briassoulis, D., Pyromali, C., Convertino, F., Schettini, E., Carroccio, S.C., Cerruti, P., Kernchen, S., Dattilo, S., Nikama, J., Soinne, H., Vox, G., Selonen, S., Löder, M.G., Laforsch, C., Mistriotis, A., 2026. Inhibition factors and soil contamination by macro/micro-particles related to biodegradation of mulching films in Mediterranean and northern climates. Polym Degrad Stabil 250, 112163.
[83] Liu, Y., Zhong, Y., Hu, C., Xiao, M., Ding, F., Yu, Y., Yao, H., Zhu, Z., Chen, J., Ge, T., Ding, J., 2023. Distribution of microplastics in soil aggregates after film mulching. Soil Ecol Lett 5.
[84] Göpferich, A., 1996. Mechanisms of polymer degradation and erosion. Biomaterials 17, 103–114.
[85] Kernchen, S., Schmalz, H., Löder, M.G.J., Georgi, C., Einhorn, A., Greiner, A., Nölscher, A.C., Laforsch, C., Held, A., 2024. Atmospheric deposition studies of microplastics in Central Germany. Air Qual Atmos Health 17, 2247–2261.